ISSN 1063-7710, Acoustical Physics, 2011, Vol. 57, No. 6, pp. 866–871. © Pleiades Publishing, Ltd., 2011.

ACOUSTIC SIGNAL PROCESSING AND COMPUTER SIMULATION

Propagation Characteristics of the Laser-Generated Lower-Order Lamb Waves in One-Dimensional Periodic Thin Plates[1]

Ding Hong-xing, Shen Zhong-hua, Jia Jing, Ni Xiao-wu

College of science, Nanjing University of Science and Technology, Nanjing 210094, China

e-mail: shenzh@mail.njust.edu.cn, dinghxing@126.com

Received May 31, 2011

Abstract—Using the finite element method (FEM), we study the thermoelastic generation and the transmitted power spectra (TPS) of Laser-generated lower-order Lamb wave mode in an one-dimensional thin aluminum plate engraved by a periodic rectangular grating. The calculation verified that the equally good Lamb waves band gaps can also exist in an one-component periodic structure and the width and location of the band gaps can be regulated by the parameters of the depth of the grooves (h), the ratio of the lattice period to the plate thickness (D/L) and the ratio of the width of the grooves to the lattice period (d/D). Specially, we suggest that Lamb wave band gaps can be substantially enlarged by using multiple periodic systems which consist of several pieces of periodic structure with different D/L.

DOI: 10.1134/S1063771011060054

1. INTRODUCTION

The bulk and surface acoustic waves propagation in elastic periodic structures have attracted increasing attention during the past few years [1–4]. The possibilities and promises of using opto-acoustic spectroscopy employing surface acoustic waves (SAW) are analyzed more than twenty years ago [5]. The existence of complete phononic band gaps, frequency ranges in which acoustic waves are forbidden to propagate, suggests many possible applications of phononic structures, such as acoustic lens, acoustic filters, and efficient waveguides.

The Lamb waves are acoustic waves propagating in thin plates with free boundaries [6]. Lamb waves are used increasingly for certain non-destructive evaluation problems, as they can propagate over long distances in plate-like structures [7]. By the results of experimental measurement of the Lamb wave s amplitude at the fundamental frequency, the spatial distributions of the quadratic and cubic nonlinear acoustic parameters can be calculated [8]. Recently, Lamb waves in phononic crystal (PC) plates have received increasing attention in the community of PC research because the released researches show that Lamb waves in two-dimensional PC plates [9–12] and one-dimensional PC plates [13–19] also exhibit complete band gaps. As a result, many efforts has devoted to the studies of Lamb wave band gaps in PC plate and their applications, such as Lamb-wave filters, Lamb-wave resonant cavities for amplification of acoustic energy.

In previous studies on Lamb waves in one-dimensional PC plates, researches are mainly focused on the two-component structures. Based on a rigorous theory of elastic wave, Chen et al. [13] have employed plane wave expansion (PWE) method and transient response analysis (TRA) to demonstrate the existence of stop bands for lower-order Lamb wave modes in 1D plate. Gao et al. [14] have developed a virtual plane wave expansion (V-PWE) method to study the substrate effect on the band gaps of lower-order Lamb waves propagating in thin plate with 1D phononic crystal coated on uniform substrate. They also studied the quasiperiodic (Fibonacci system) 1D system and find out the existence of split in phonon band gap [15]. In order to reduce the computational complexity without losing the accuracy, Zhu et al. [16] have promoted an efficient method named harmony response analysis (HRA) and supercell plane wave expansion (SC PWE) to study the behavior of Lamb wave in silicon-based 1D composite plates. Zou et al. [17] have employed V-PWE method to study the band gaps of plate-mode waves in 1D piezoelectric composite plates with substrate. The objects of above studies are all two-component structures and three-component periodic [18] and quasiperiodic [19] composite thin plates are also investigated since it has more and better options to achieve the complete gaps.

On the other hand, for the Lamb waves are very sensitive to the surface state, an one-component structure with periodic surface can also exhibit band gaps for low-order Lamb wave modes. M. Bavencoffe et al. [20] have studied the propagation of Lamb wave on an aluminium plate engraved by a periodic sinusoidal grating and established the relation between the depth of the grooves and the width of the forbidden bands. Obviously, one-component structure with periodic

[1] The article is published in the original.

surface can be made easier than two or three-component PC. Therefore, it has significant importance to study in detail the propagation of Lamb waves in one-dimensional thin plate with periodic surface. In this paper, the case of an aluminium plate with rectangular grating on the top surface is studied. Firstly, the thermoelastic theory and rigorous elastic wave theory for the generation and propagation of Laser-generated Lamb waves are presented. Secondly, we study the influence of the depth of the grooves (h), the ratio of the lattice period to the plate thickness (D/L) and the ratio of the width of the grooves to the lattice period (d/D) on the width and location of the band gaps by calculating the TPS with the FEM. Finally, we suggest that Lamb wave band gaps in one-dimensional periodic thin plate can be substantially enlarged by using multiple structures which consist of several pieces of periodic structure with different D/L.

2. THEORETICAL MODEL

2.1. Theory of Transient Temperature Field Generation

The analytical material adopt the Al plate engraved by a periodic rectangular grating on the top surface, which is illuminated by a laser line source in normal direction at $x = 0$. Because the dimension of the grooves and the energy distribution of the laser beam is uniform in the y axis direction, meanwhile the incident waves are assumed to be polarized on the x–z plane, and all deformations are independent of y. Thus the problem can be formulated in two dimensions on the x–z plane as shown in Fig. 1. We suppose that the computed rectangular grating has a period of D, in which the groove width is d. The thickness of the plate and the depth of the groove are L and h, respectively. The first structure as shown in Fig. 1a has a single period of D and the second one as shown in Fig. 1b is made of two substructures with period D_1 and D_2, respectively. The spatial of the laser beam is assumed to be Gaussian mode in the x-axis so that a two-dimensional Cartesian coordinates is adopted. The thermal conduction equation can be described as:

$$\rho c\frac{\partial T(x,z,t)}{\partial t} = \frac{\partial}{\partial x}\left(k_x\frac{\partial T(x,z,t)}{\partial x}\right) + \frac{\partial}{\partial z}\left(k_z\frac{\partial T(x,z,t)}{\partial z}\right), \quad (1)$$

where $T(x, z, t)$ represents the temperature distribution at time t; and ρ, c, k_x and k_z are the density, specific heat at constant pressure, and thermal conductive coefficients in x-, z-directions, respectively.

The normal boundary conditions are listed as follows:

$$-k_z\frac{\partial T(x,z,t)}{\partial z}\bigg|_{z=L} = I_0A(T)f(x)g(t) \quad (2)$$

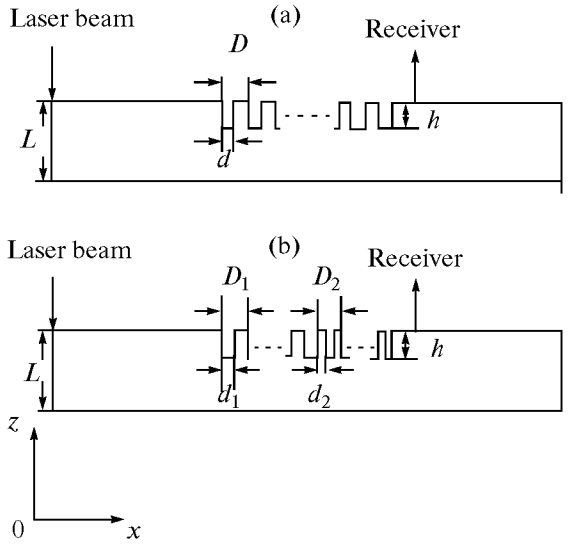

Fig. 1. Schematic diagram of the laser irradiating periodic plate. (a) Single periodic system. (b) Multiple periodic system.

$$\text{and } \frac{\partial T(x,z,t)}{\partial z}\bigg|_{z=0} = 0, \quad (3)$$

where $A(T)$ is the optical absorptivity of the specimen surface, I_0 is the incident laser power density, and $f(x)$ and $g(t)$ are the spatial and temporal distributions of the laser pulse, respectively. These two functions can be written as:

$$f(x) = \exp\left(-\frac{x^2}{a_0^2}\right), \quad g(t) = \frac{t}{t_0}\exp\left(-\frac{t}{t_0}\right), \quad (4)$$

where a_0 is the half-width of the line souse, and t_0 is the rise time of the laser pulse.

2.2. Theory of Laser Ultrasound Generation by the Thermoelastic Mechanism

When the specimen surface is illuminated with a laser pulse with the energy less than the melting threshold of the specimen, a transient displacement field will be excited due to thermoelastic expansion. In an isotropic body, the displacement satisfies

$$(\lambda + 2\mu)\nabla(\nabla \cdot U) - \mu\nabla \times \nabla \times U - \alpha_l(3\lambda + 2\mu)\nabla T(x,z,t) = \rho\frac{\partial^2 U}{\partial t^2}, \quad (5)$$

where $U = U(x, z, t)$ is the time-dependent displacement, λ and μ are the Lame' constants, ρ is the density, and α_l is the thermoelastic expansion coefficient of the isotropic plate material. The boundary conditions at the two parallel surfaces $z = 0$ and $z = L$ are

Properties of aluminum used in the calculation

Absorptivity	$A(T) = 5.2 \times 10^{-2} + 3 \times 10^{-5}(T-300)$
Thermal conductive coefficient K, W m^{-1} K^{-1}	292.6, $T < 200$ K
	$249.45 - 0.085T$, 200 K $< T <$ 730 K
	$198.47 - 0.014T$, 730 K $< T < T_m$
Density ρ, kg m^{-3}	$-0.22T + 2769$, 300 K $< T < T_m$
Thermal capacity C, J kg^{-1} K^{-1}	$3.791T$, $T < 200$ K
	$780.27 + 0.488T$, 200 K $< T < T_m$
Poisson's ratio	0.34
Young's modulus, Pa	7.02×10^{10}
Thermal expansion coefficient, K^{-1}	2.31×10^{-5}

$$\hat{n} \cdot \lfloor \sigma - (3\lambda + 2\mu)\alpha T(x, z, t)\hat{I} \rfloor = 0, \quad (6)$$

where $\hat{n}$ is the unit vector normal to the surface, $\hat{I}$ is the unit tensor, and σ is the stress tensor. In addition to the boundary condition, there is also an initial condition

$$U(x, z, t) = \frac{\partial U(x, z, t)}{\partial t} = 0, \quad t = 0. \quad (7)$$

2.3. Numerical Method

The classical thermal conduction equation for finite element model can be expressed as:

$$[K]\{T\} + [C]\{\dot{T}\} = \{p_1\} + \{p_2\}, \quad (8)$$

with the heat capacity matrix $[C]$, the conductivity matrix $[K]$, the heat flux vector $\{p_1\}$ and the heat source vector $\{p_2\}$, where $\{T\}$ is the temperature vector, $\{\dot{T}\}$ is the temperature rate vector. For wave propagations, and ignoring damping, the governing finite element equations are:

$$[M]\{\ddot{U}\} + [S]\{U\} = \{F_{ext1}\}, \quad (9)$$

where $[M]$ is the mass matrix, $[S]$ is the stiffness matrix, $\{U\}$ is the displacement vector, $\{\ddot{U}\}$ is the second time derivative of the displacement vector, represents acceleration vector and $\{F_{ext}\}$ is the external force vector. For thermoelasticity, the external force vector for an plane element is $\int_{S_e} [B]^T [D]\{\varepsilon_0\} dS$, where $\{\varepsilon_0\}$ is the thermal strains vector, $[B]^T$ is the transpose of the derivative of the shape functions and $[D]$ is the material matrix.

3. NUMERICAL RESULTS AND DISCUSSIONS

3.1. Laser and Materials Parameters

Based on the above-described theories, the thermoelastic generation and propagation of Lamb waves are calculated in thin aluminum plates as shown in Fig. 1 with 220 mm length and 0.5 mm thickness, respectively. The line laser pulse with a spatial Gaussian distribution and the energy, the pulse rise time and the half-width of it are taken to be 13.5 mJ, 10 ns and 300 μm, respectively. The thermophysical and mechanical properties of aluminum in the calculation are listed in the table, where T_m is the melting point of the material.

3.2. Transmitted Power Spectrum (TPS) by Finite Element Method (FEM)

In order to demonstrate the existence of the band gaps for the lower-order Lamb wave in the 1D periodic structure, the FEM is employed to calculate the TPS for the finite periodic structure. As shown in Fig. 1, Lamb wave are excited by a perpendicularly incident laser line source at $x = 0$ and received at the point 10 mm away from the last groove. The generation source is 100 mm from the first groove in order to obtain approximate plane waves when the wave fronts reach it. For the frequency spectrum of the laser-exited acoustic wave is defined by the Fourier transform of the spatial distribution of heat source [21], the received vertical displacement in time domain can be easily Fourier transformed to yield the TPS. The finite element models are constructed accordingly. The minimum element size near the affected zone is 10 μm, whereas the element size outside the heat-affected zone is 100 μm and the time step size is 10 ns. The step sizes of temporal and spatial discretizations in the FE calculations are fine enough to meet the demand of the accuracy of generated ultrasound propagation.

Firstly, we study the influence of the ratio of d/D on the band gap. Figures 2a depicts the TPS for the cases of $L = 0.5$ mm, $h = 0.2$ mm, $D/L = 2$ and $d/D = 0.4$, 0.5, 0.6, respectively. For comparison, the TPS for a pure aluminium plate of 0.5 mm thickness is also shown (dashed line). Figures 2a shows that there are two obvious band gaps in the structure of $d/D = 0.4$, 0.5, and 0.6, the first is an incomplete forbidden gap and the second is the lowest complete forbidden gap. One can easily find that the initial frequencies of the

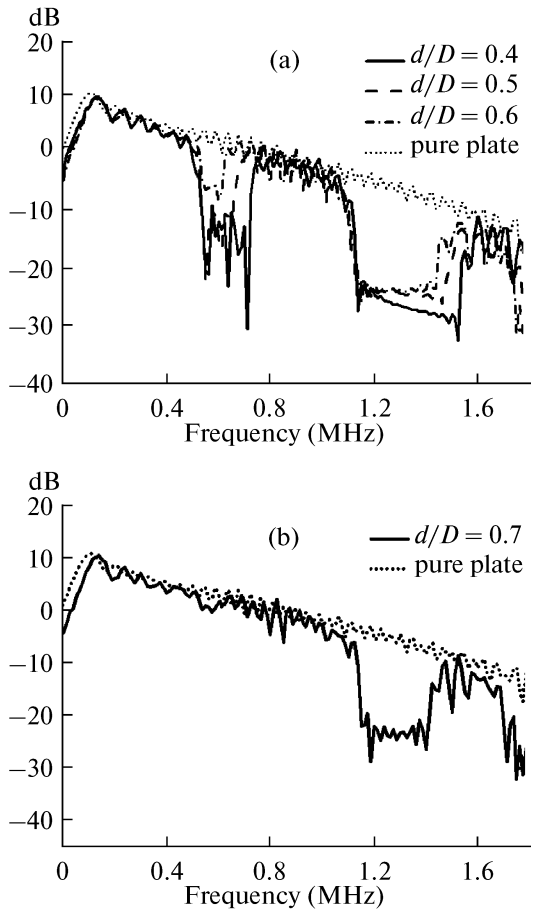

Fig. 2. The TPS computed by the FEM for the first system in Fig. 1; $h = 0.2$ mm, $L/D = 0.5$ and (a) $d/D = 0.4$, 0.5, 0.6, (b) $d/D = 0.7$, respectively.

two band gaps are almost constant and the value are about 540 and 1110 kHz, respectively, and the ending frequency shifts toward the low frequency with the width of grooves increase, that is to say that the width of band gap decrease with the width of grooves increase. When $d/D = 0.7$ (Figs. 2b), more interesting things happen, the incomplete forbidden gap disappears almost completely.

Furthermore, in order to investigate the influence of the depth of the grooves on the band gaps, we calculate the TPS for the periodic plate with $L = 0.5$ mm, $D/L = 2$, $d/D = 0.5$, and $h = 0.1$ and 0.2 mm, respectively. The results are shown in Fig. 3, which tells us that the width and the midgap frequency of the forbidden gaps are related to the depth of the grooves: the first complete band gap of $h = 0.2$ mm is larger and with lower midgap frequency than that of $h = 0.1$ mm.

Lastly, we show the dependence of TPS on D/L. Figure 4 depicts the TPS for the 1D periodic plate with $L = 0.5$ mm, $h = 0.2$ mm, $d/D = 0.5$, and $D/L = 2$ and 2.4, respectively. Two band gaps are clearly seen in the periodic system and, for $D/L = 2.4$, the first band extends from frequency about 360 up to 460 kHz and

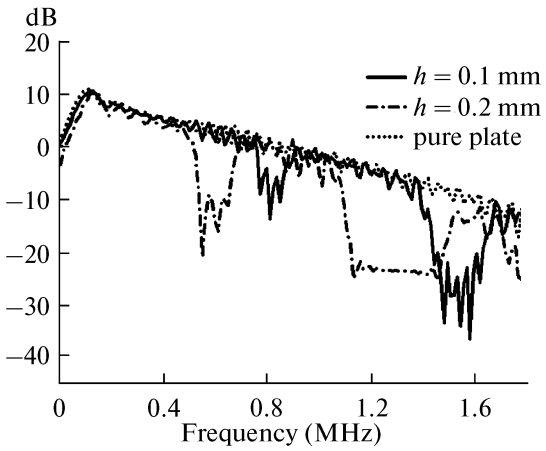

Fig. 3. The TPS computed by the FEM for the first system in Fig. 1; $L/D = 0.5$, $d/D = 0.5$, and $h = 0.1$ and 0.2 mm, respectively.

the second one from about 860 up to 1185 kHz. In the case of $D/L = 2$, the two band gaps extend from about 540 to 690 kHz and 1110 to 1535 kHz, respectively. The results tell us that the band gaps become narrow and shift toward the lower frequency with the D/L increase.

Figure 5 presents the complete evolution of the Lamb wave band structure with the filling fraction d/D, the depth of the grooves h and the ratio of the lattice period to the plate thickness D/L. Figure 5a depicts the structure of the low-frequency gap as a function of the d/D. In the calculation, $h = 0.2$ mm and $D/L = 2$. As the d/D increases, the maximum frequencies of two forbidden gaps move down monotonously and linearly and the minimum frequency of the incomplete band gap is constant, however, the minimum frequency curve of the lowest complete band gap fall firstly and then rise from $d/D = 0.5$ with a very

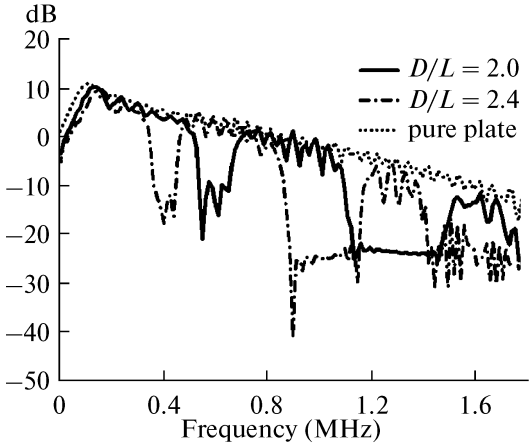

Fig. 4. The TPS computed by the FEM for the first system in Fig. 1; $h = 0.2$ mm, $d/D = 0.5$, and $D/L = 2$ and 2.4, respectively.

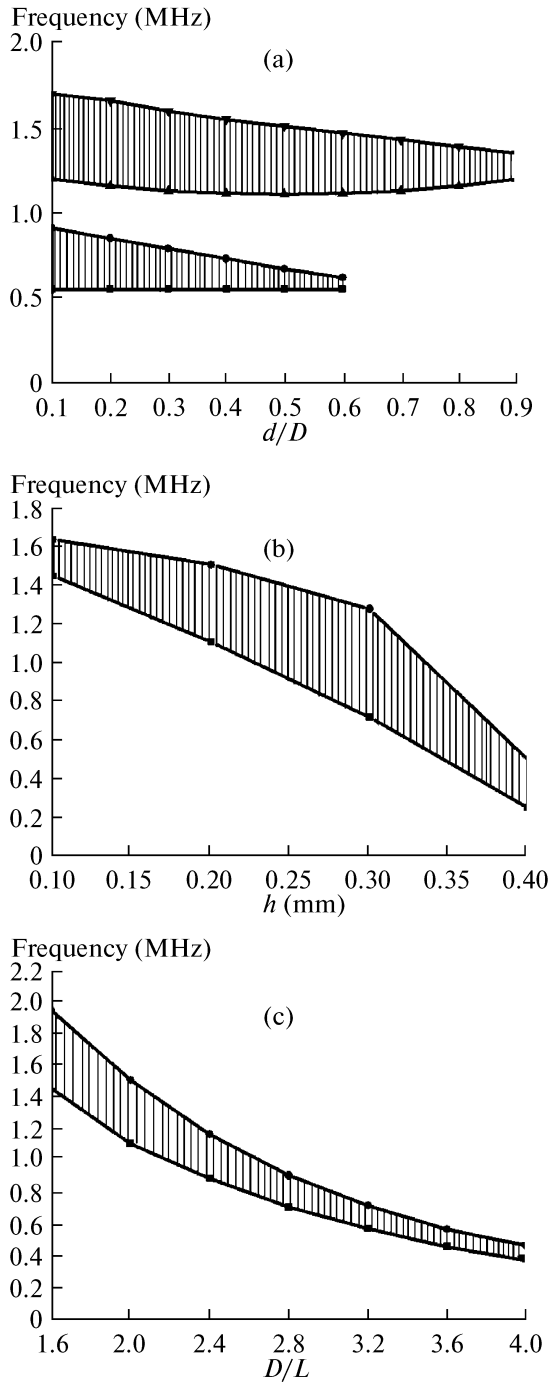

Fig. 5. The complete evolution of the low-frequency Lamb wave band gap with different physical parameters: (a) the d/D, (b) the h, and (c) the D/L.

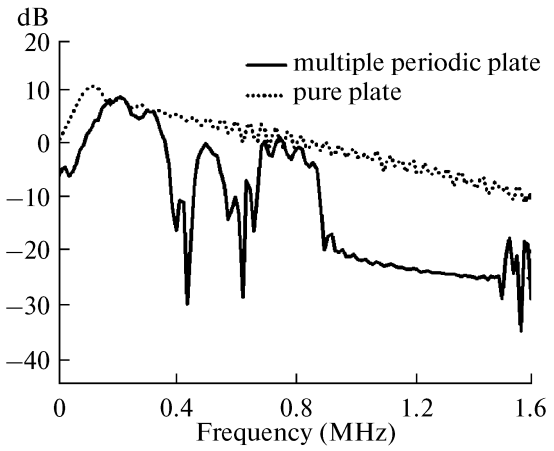

Fig. 6. The TPS computed by the FEM for the second system in Fig. 1; $h = 0.2$ mm, $d_1/D_1 = d_2/D_2 = 0.5$, $D_1/L = 2$, and $D_2/L = 2.4$, respectively.

good symmetry. Thus, the width of incomplete forbidden gap decreases gradually and disappears as d/D is greater than 0.7. Figure 5b displays the depth of the grooves dependence of the lowest complete band gap width. In the numerical simulation, the $L = 0.5$ mm, $D = 1$ mm, and d/D is fixed at 0.5. From the panel, it can be seen that the minimum frequencies of the forbidden gap move down monotonously and linearly and the width of the gap increase firstly and then decrease with the grooves become deeper. Figure 5c presents the complete evolution of the lowest frequency band gap with D/L. In the calculation, $h =$ 0.2 mm and $d/D = 0.5$. In the panel, it can be easily seen that the maximum and minimum frequencies of the first complete lamb wave band gap and the width of it move down monotonously and reaches them maximum and minimum value when D/L is 1.6 and 4, respectively.

The simulated TPS for the structure of Fig. 1b is shown in Fig. 6. For which, $L = 0.5$ mm, $h = 0.2$ mm, $d_1/D_1 = d_2/D_2 = 0.5$, $D_1/L = 2$, and $D_2/L = 2.4$, respectively. The result shows that three band gaps exist in the systems and the first gap extends from the frequency about 370 up to 460 kHz, the second from about 540 up to 675 kHz and the third one is a broad region from about 875 up to 1525 kHz. It can be found that the frequency range of non-transmission can be essentially enlarged as desired by using two substructures with different period to form a multiple system. In principle, each substructure has its own band gap and the band structure of Lamb waves are strongly affected by the ratio of D/L. If the band gaps of the two substructures are overlapped in a certain frequency range, the forbidden transmission frequency range of the multiple periodic system will be from the lowest edge of the non-transmission range to the highest upper edge of the non-transmission ranges of the constituent periodic plates. As a result, the frequency range of non-transmission is in some sense enlarged.

4. CONCLUSIONS

The FEM is applied to the numerical calculation for the thermoelastic generation and propagation of the lowest order Lamb waves (symmetric mode s_0 and

antisymmetric mode a_0) excited by a pulsed laser in a periodic thin plate. The received vertical displacement in time domain can be Fourier transformed to yield the TPS for the finite systems. The results show that the forbidden band gaps exist obviously and its structure depends strongly on three parameters, namely, d/D, h, and D/L. Thus, we can achieve the needed structure of band gaps for Lamb wave by varying the critical parameters of the plate. Particularly, the Lamb wave band gaps can be essentially enlarged as desired by using two substructures with overlapping band gaps to form a multiple periodic system, which implies some potential applications in the future.

ACKNOWLEDGMENTS

Authors would like to thank the financial support of this research from the National Science Foundation of China under nos. 60778006 and 60878023, and the Program for New Century Excellent Talents in University (NCET).

REFERENCES

1. Takashi Aono and Shin-ichiro Tamura, Phys. Rev. **58**, 4838 (1998).
2. R. E. Vines, J. P. Wolfe, and A. V. Every, Phys. Rev. B **60**, 11871 (1999).
3. Y. Tanaka, Y. Tomoyasu, and S. I. Tamura, Phys. Rev. B **62,** 7387(2000).
4. Tsung-Tsong Wu, Zin-Chen Hsu, and Zi-Gui Huang, Phys. Rev. **71**, 064303 (2005).
5. A. A. Karabutov, Sov. Phys. Usp. **28**, 1042 (1985).
6. A. I. Korobov and M. Yu. Izosimova, Acoust. Phys. **52,** 589 (2006).
7. I. A. Viktorov, *Rayleigh and Lamb Waves: Physical Theory and Applications* (Plenum, New York, 1967).
8. M. Yu. Izosimova, A. I. Korobov, and O. V. Rudenko, Acoust. Phys. **5**, 153 (2009).
9. B. Bonello, Ch. Christine, and F. Ganot, Appl. Phys. Lett. **90**, 021909 (2007).
10. Jia-Hong Sun and Tsung-Tsong Wu, Phys. Rev. **76**, 104304 (2007).
11. Tzung-Chen Wu, Tsung-Tsong Wu, and Jin-Chen Hsu, Phys. Rev. **79**, 104306 (2009).
12. Jiu-Jiu Chen and B. Bonello, Phys. Rev. E **78**, 036609 (2008).
13. Jiu-Jiu Chen, Kai-Wen Zhang, Jian Gao, and Jian-Chun Cheng, Phys. Rev. **73**, 094307 (2006).
14. Jian Gao and Jian-Chun Cheng, Appl. Phys. Lett. **90**, 111908 (2007).
15. Jian Gao, Xin-Ye Zou, Jian-Chun Cheng, and Baowen Li, Appl. Phys. Lett. **92**, 023510 (2008).
16. Xue-feng Zhu, Tao Xu, Sheng-chun Liu, and Jian-chun Cheng, J. Appl. Phys. **106**, 104901 (2009).
17. Xin-ye Zou, Bin Liang, Qian Chen, and Jian-chun Cheng, IEEE Trans. Ultrason. Ferroelectr. Freq. Control **56**, 361 (2009).
18. Jiu-Jiu Chen, H. L. W. Chan, and Jian-Chun Cheng, Phys. Lett. A **366**, 493 (2007).
19. Jiu-Jiu Chen, Qiong Wang, and Xu Han, Mod. Phys. Lett. B **24**, 161 (2010).
20. M. Bavencoffe, A.-C. Hladky-Hennion, B. Morvan, and J.-L. Izbickil, IEEE Trans. Ultrason. Ferroelectr. Freq. Control **56**, 1960 (2009).
21. V. E. Gusev and A. A. Karabutov, *Laser Optoacoustics* (AIP, New York, 1993).